# Multiple actions of φ-LITX-Lw1a on ryanodine receptors reveal a functional link between scorpion DDH and ICK toxins

Jennifer J. Smith[a], Irina Vetter[a], Richard J. Lewis[a], Steve Peigneur[b], Jan Tytgat[b], Alexander Lam[c], Esther M. Gallant[c], Nicole A. Beard[d], Paul F. Alewood[a,1,2], and Angela F. Dulhunty[c,1,2]

[a]Chemical and Structural Biology, Institute for Molecular Biosciences, University of Queensland, St. Lucia, QLD 4072, Australia; [b]Laboratory of Toxicology, University of Leuven, 3000 Leuven, Belgium; [c]Department of Molecular Bioscience, John Curtin School of Medical Research, Australian National University, Canberra, ACT 2601, Australia; and [d]Discipline of Biomedical Sciences, Faculty of Education, Science, Technology and Mathematics, University of Canberra, Canberra, ACT 2601, Australia

We recently reported the isolation of a scorpion toxin named $U_1$-liotoxin-Lw1a ($U_1$-LITX-Lw1a) that adopts an unusual 3D fold termed the disulfide-directed hairpin (DDH) motif, which is the proposed evolutionary structural precursor of the three-disulfide-containing inhibitor cystine knot (ICK) motif found widely in animals and plants. Here we reveal that $U_1$-LITX-Lw1a targets and activates the mammalian ryanodine receptor intracellular calcium release channel (RyR) with high (fM) potency and provides a functional link between DDH and ICK scorpion toxins. Moreover, $U_1$-LITX-Lw1a, now described as φ-liotoxin-Lw1a (φ-LITX-Lw1a), has a similar mode of action on RyRs as scorpion calcines, although with significantly greater potency, inducing full channel openings at lower (fM) toxin concentrations whereas at higher pM concentrations increasing the frequency and duration of channel openings to a submaximal state. In addition, we show that the C-terminal residue of φ-LITX-Lw1a is crucial for the increase in full receptor openings but not for the increase in receptor subconductance opening, thereby supporting the two-binding-site hypothesis of scorpion toxins on RyRs. φ-LITX-Lw1a has potential both as a pharmacological tool and as a lead molecule for the treatment of human diseases that involve RyRs, such as malignant hyperthermia and polymorphic ventricular tachycardia.

The correct regulation and interpretation of chemical signals in the body is a critical process underpinning all normal physiological functions. For a signal to elicit a biological response it must first be transmitted from the exterior of a cell to its interior, upon which a cascade of events is triggered. An increase in the cytosolic concentration of calcium is often a key step in the transduction of intracellular signals. Large amounts of calcium are stored in the endoplasmic reticulum and sarcoplasmic reticulum (SR) (1), and intracellular calcium levels can be rapidly increased through release from these organelles. In muscle cells, calcium release is essential to the process of muscle contraction and occurs via the opening of channels located on the SR known as ryanodine receptors (RyRs) (2). RyRs are the largest known ion channel, adopting a homotetrameric structure more than 2 million Da in mass (3). Mammals have three RyR isoforms that are widely expressed in a range of both excitable and nonexcitable cells. Despite their prevalence in a variety of tissues, RyR1 is commonly referred to as the skeletal subtype and RyR2 the cardiac subtype. This nomenclature is reflective of the muscle tissues from which they were first isolated and also the predominant subtype found in these tissues (4, 5). RyR3 was initially discovered in the brain (6) and seems to be the most broadly expressed of the three subtypes (7).

Because RyRs are of central importance in muscular excitation–contraction coupling, aberrations in the function of these ion channels result in medically significant disorders. Many mutations in RyRs have been linked to potentially fatal disorders, such as malignant hyperthermia and catecholaminergic polymorphic ventricular tachycardia (8, 9). Aside from genetic mutations, atypical posttranslational modifications of RyRs, including hyperphosphorylation and S-nitrosylation, have been implicated in heart failure and pathologic muscle fatigue (10–12). Because of their wide distribution, there is mounting evidence to suggest that dysregulation of RyRs also plays a role in a plethora of other disease states, including chronic pain, neurodegenerative disorders such as Alzheimer's disease, and intellectual deficit (13–15). The contribution of misregulated or abnormal RyR activity over such a broad range of disorders means that establishing the precise involvement of RyRs in disease states has become an emergent and exciting field of study.

Pharmacological tools such as the classic activator caffeine and ryanodine, the plant-derived alkaloid modulator of RyRs, have enabled research into the behavior of RyRs in vitro (16, 17). It was discovered that ryanodine and its congeners, collectively termed ryanoids, were able to induce long-lived subconductance states in RyRs, whereby the amplitude of the current is less than maximal so that the channel seems to be partially open (18, 19). Another group of RyR modulators are the calcines, which are peptidic toxins found in scorpion venoms. Originally isolated from the scorpion *Pandinus imperator*, imperatoxin A (IpTxA) is the best characterized of the calcines, with low μM IpTxA concentrations inducing RyR substates and inhibiting full single channel current opening. Interestingly, low nM IpTxA concentrations activate RyR by increasing transient activity and the probability of full channel openings (20, 21). This apparent incongruity is believed to be due to the existence of two or more ligand-binding sites on RyRs. It is thought IpTxA binds at a high-affinity site causing activation, whereas subconductance states arise on occupancy of lower-affinity sites (21). Other calcines, such as maurocalcine and hadrucalcin, demonstrate similar activities (22, 23). Their ability to modulate RyR activity makes calcines potential drug leads for the treatment of RyR diseases in humans. In addition, calcines are membrane permeable, and this property is attractive for broad therapeutic use and may be exploited to deliver drugs intracellularly. Indeed, a pharmacologically inert, disulfideless analog of maurocalcine has been used as a carrier molecule to transport compounds into cells (24).

All calcines adopt a 3D fold called the inhibitory cystine knot (ICK), a structural motif characterized by two disulfide bonds pierced by a third to form a pseudoknot (25). Although common in a variety of organisms ranging from spiders to plants (26), ICK peptides are rare in scorpion venoms, and most scorpion toxins are folded into the cystine-stabilized αβ (CSαβ) motif, consisting of an α helix connected to three antiparallel β-sheets via three or four disulfide bonds (27). There is considerable evidence to suggest CSαβ scorpion toxins evolved through the recruitment and subsequent neofunctionalization of hemolymphatic CSαβ insect defensins (28). However, the origin of ICK peptides in scorpion venoms is not as thoroughly delineated, although genomic evidence suggests a common evolutionary origin for ICK peptides in animals (29).

It has been proposed that the ICK motif arose through elaboration of a simpler, two-disulfide bonded fold termed the disulfide-directed hairpin (DDH) (30). We recently validated the existence of this previously hypothetical fold with the discovery and structural characterization of a scorpion toxin named φ-liotoxin-Lw1a (φ-LITX-Lw1a; hereafter LITX), a native example of a DDH peptide (31). Because all non βαββ-containing ICK-folded scorpion toxins characterized thus far target RyRs (25), we hypothesized that LITX would also affect RyRs. The present study not only confirms this hypothesis but also demonstrates that LITX modifies RyR activity in a similar manner as IpTxA, reinforcing the concept of an evolutionary link between ICK and DDH scorpion peptides. Additionally, we designed and synthesized an analog of LITX that lost the ability to activate RyRs while retaining the capability for substate induction. The actions of the mutant LITX provides further support for the presence of at least two different binding sites on RyRs.

## Results

### Synthesis and Structural Characterization of LITX W36A Mutant.

The W36A LITX mutant was synthesized by solid-phase peptide chemistry and oxidized to one major peak (Fig. S1*A*). The disulfide bond connectivity was ascertained by tryptic digestion and mass spectrometric analysis of the oxidized peptide. The cysteine residues were found to be unambiguously arranged in a 1–3, 2–4 connectivity via mass spectrometric analysis of trypsin-digested fragments of the oxidized peptide, which maintains the same disulfide bond connectivity as the wild-type toxin (Fig. S2). Analysis of the fully folded mutant peptide by NMR spectroscopy revealed the secondary Hα shift plot to be very similar to that of the native peptide, indicating the overall fold of the mutant and wild-type toxins to be identical (Fig. S1*B*).

### LITX Is a Highly Potent and Selective Modulator of RyR1 and RyR2.

LITX applied to the cytoplasmic side of RyRs activated the channels (Fig. 1 *A* and *B*). The effect of the toxin on the current flowing through RyR channels was measured as the probability of channel opening to all levels that exceeded baseline noise (and were greater than 15–20% of the maximal conductance), that is, the fraction of the total recording time that the channels were open. Application of 10–100 fM LITX increased RyR2 and RyR1 open probability (Fig. 1 *C* and *D* and Table S1). LITX increased the duration of RyR2 and RyR1 openings and decreased the time spent in the closed state (Table S1).

In control experiments, LITX in the luminal solution did not enhance RyR2 activity (Fig. 1*E*, $n = 5$); indeed, there was a trend toward reduced activity. TFA present with the peptide was not responsible for increasing activity: TFA from 200 pM to 20 nM had no effect on RyR1 (Fig. 1*F*, $n = 5$). LITX in the bilayer solution in the absence of RyRs did not induce channel activity ($n = 3$). Finally, 100 pM LITX added to the cytoplasmic side of RyR1 blocked by ruthenium red did not increase activity ($n = 3$). [³H]Ryanodine binding was used as an additional measure of the effect of LITX on RyRs (Fig. 1 *G* and *H*), and it was found that ≥10 fM LITX increased [³H]ryanodine binding. The error bars on the relative $P_o$ of RyR1 are large (Fig. 1*D*). This is likely due
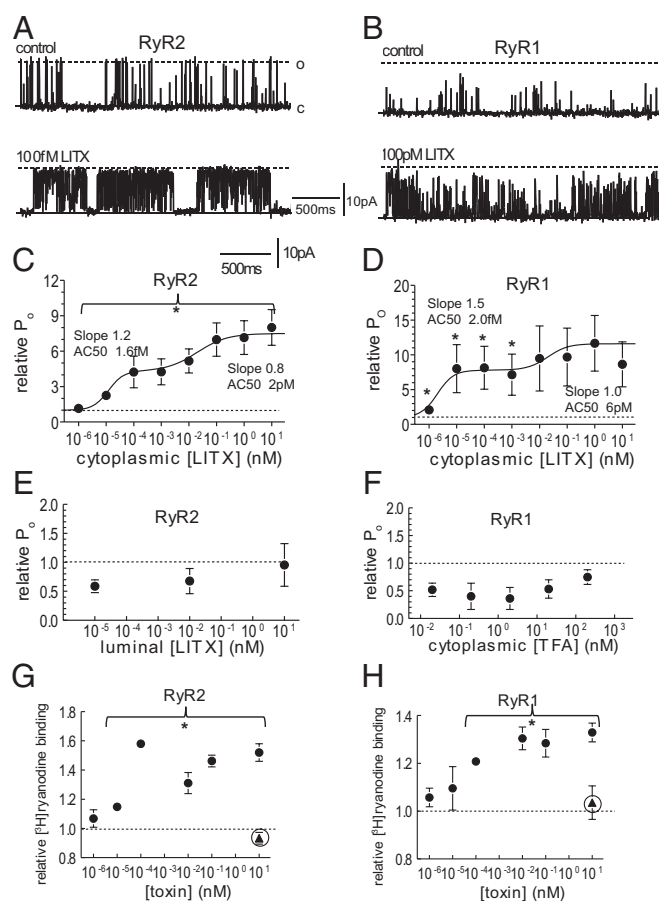


**Fig. 1.** Activity of the wild-type LITX on RyR2 and RyR1 channels. (*A* and *B*) Single RyR2 (*A*) and RyR1 (*B*) currents recorded at +40 mV with channel opening upward from the closed current level (solid line labeled c), to maximum open current (broken line labeled o). (*C* and *D*) Average relative open probability ($P_oT/P_oC$; *Materials and Methods*) ($n = 5$–12) after application of wild-type LITX at indicated concentrations. Average data in *C* and *D* include measurements obtained at +40 mV and −40 mV, because no voltage dependence of effects was seen. The curves through the data in *C* and *D* are the sum of two Hill equations with constants given in the figure and in the text. (*E*) Average relative open probability of RyR2 channels exposed to LITX in the luminal solution ($n = 5$). (*F*) Average relative open probability of RyR1 channels after adding TFA to the cytoplasmic solution ($n = 5$). (*G* and *H*) Average relative [³H]ryanodine binding ($n = 3$–6) to RyR2 and RyR1 channels in SR vesicles after adding wild-type LITX (filled circles) and W36A (filled triangles). Data in *C*–*G* are shown as mean ± 1 SEM. *Significant change at indicated concentrations.

to variability between channels in the summed effects of a decline in maximal conductance and increase in submaximal conductance opening (Fig. 2*D*). Variability between individual channels is a feature of RyRs and is well documented (32, 33).

Curves through the relative $P_o$ data (Fig. 1 *C* and *D*) were fitted to the sum of two Hill equations. The [toxin] for activation to 50% (AC$_{50}$s) of the first equations are 1.6 fM (RyR2) and 2.0 fM (RyR1) and the Hill coefficients are 1.2 and 1.5, respectively. The second equations have AC$_{50}$s of 2.0 pM (RyR2) and 6.0 pM (RyR1) and Hill coefficients of 0.8 and 1.0, respectively. The first component corresponds to the increase in full conductance openings (Fig. 1 *A* and *B*). The second likely reflects increased substate (or subconductance) openings [i.e., openings to levels less than the maximum conductance (Fig. 2) and maintained for >2 ms (and not an artifact of filtering)]. Although substate openings of RyRs occur constitutively (21), the number and duration of openings increased with higher LITX concentrations
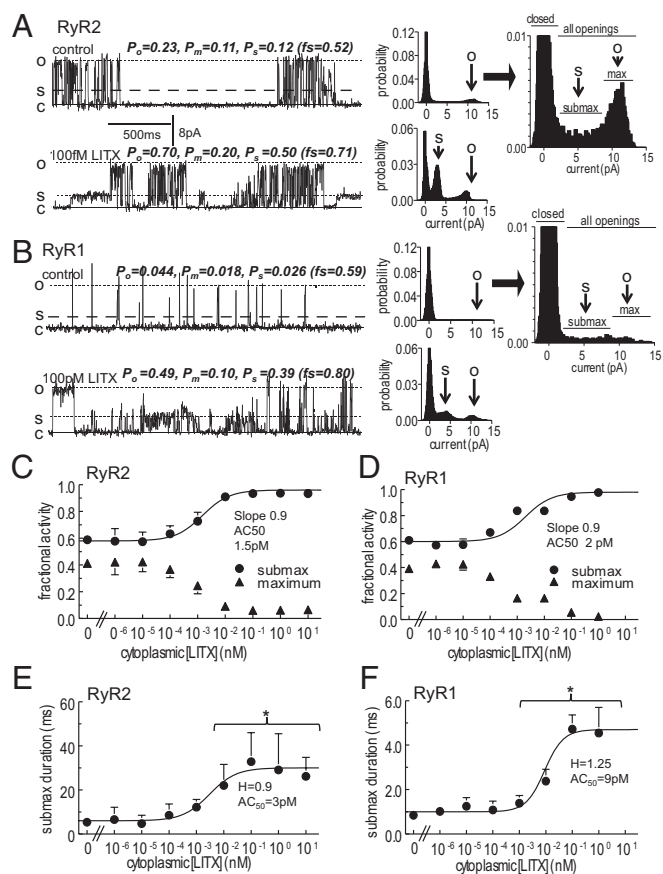
**Fig. 2.** Subconductance openings of RyR channels are prolonged by exposure to LITX. (*A* and *B*) (*Left*) Single RyR2 (*A*) and RyR1 (*B*) currents at +40 mV, showing prolonged substate openings after addition of LITX at indicated concentrations. Parameter values with each record are for: all openings ($P_o$); maximal openings ($P_m$); substate openings ($P_s$); fraction of openings to substate levels (fs = $P_s/P_o$) (plotted in *C* and *D*). (*Center*) All points histograms. The arrow O indicates the full conductance level, and S points to the predominant substate current level. (*Right*) Histograms for control data, enlarged to illustrate which points fall into the closed bins and which fall into submaximal (submax) or maximal (max) open bins. (*C* and *D*) Fraction of openings to substate levels (circles) and to the maximum conductance (triangles). (*E* and *F*) Duration of submaximal openings. The curves through the data in *C–F* were calculated using a Hill equation with constants given in the figure, and data are shown as mean ± 1 SEM. For visual clarity, only one error bar is shown for some data points. *Significant difference between control data and data in the presence of the toxin.

(Fig. 2 *A–F*). The probability of all openings to submaximal levels ≥15–20% of maximum current ($P_s$) was measured as the difference between the probability of openings to all current levels ($P_o$) and to the maximum level ($P_m$), [i.e., ($P_o - P_m$) as in Fig. 2]. The fraction of channel openings to submaximal levels (fs = $P_s/P_o$) increased with LITX ≥100 fM, and the fraction of openings to the full conductance declined. Although $P_o$ increased between 1 and 100 fM (Fig. 1 *C* and *D*), the fraction of openings to submaximal and maximal levels remained constant at these lower toxin levels (Fig. 2 *C* and *D*). The Hill curves indicate that LITX concentrations of 1.5 pM (RyR2) and 2.0 pM (RyR1) are the AC50s for increased submaximal openings, and the Hill coefficient for both curves is 0.9, notably similar to the second component in the relative $P_o$ fit (Fig. 1 *C* and *D*). Submaximal events in control activity indicate a range of substate levels that are maintained for ≥2ms, as well as brief events that may be larger events reduced in amplitude by filtering. With LITX there is one dominant substate level that is often maintained for >100 ms (Fig. 2 *A* and *B*). This is

reflected in the increased duration of openings at higher LITX concentrations (Fig. 2 *E* and *F*), which occurred in addition to an increase in the frequency of events (Table S2). There was no increase in submaximal activity with TFA ($n = 5$) or with addition of LITX to the luminal solution ($n = 3$).

To investigate the selectivity of LITX, the toxin was screened against a range of oocyte-expressed recombinant channels, including Na_v, K_v and Ca_v subtypes, as detailed in *SI Materials and Methods*. LITX was also applied to neonatal rat dorsal root ganglia (DRG) neurons, because animal toxins often act on receptors present on sensory nerves. DRG neurons were used as a screening tool because they contain a plethora of well-described receptors and channels, as well as many that remain to be characterized (34–36). No toxin effect was observed in any of the recombinant receptors tested or in the DRG neurons (Figs. S3 and S4).

**LITX W36A Mutant Stabilizes Mammalian RyR Substates but Does Not Cause Activation.** The C-terminal mutant LITX W36A did not increase the overall open probability of cardiac RyR2 at 10 fM to 100 pM (Fig. 3*A*) nor skeletal RyR1 at 100 pM to 100 nM (Fig. 3*B*). Indeed, as opposed to the wild-type toxin, the mutant caused a small decrease in the overall open probability in most RyR2 channels. LITX W36A also did not increase [$^3$H]ryanodine binding at 1 nM in a [$^3$H]ryanodine binding assay (triangles in Fig. 1 *G* and *H*), supporting the single channel analysis data. In contrast, the ability of LITX W36A to enhance openings to subconductance levels and to depress the fraction of openings to the maximum conductance at higher concentrations was retained (Fig. 3 *C–F*). It is likely that the reduced open probability in the average data (Fig. 3 *A* and *B*) was due to the decline in full conductance openings, which is apparent in the single channel recordings from both RyR1 and RyR2.

## Discussion

**Functional Link Between ICK and DDH Scorpion Peptides.** LITX is the most potent peptidic modulator of RyRs discovered to date and affects the activity of both RyR1 and RyR2. The potency of LITX for the high-affinity site on RyR channels in the fM range is remarkably high, being ~50,000 times greater than that of IpTxA (21) and 1,000 times higher than binding of a saxitoxin analog (zetikitoxin) to voltage-dependent sodium channels in the brain (37). Low toxin concentrations increased the probability of full channel opening, and concentrations ~100-fold higher inhibited the occurrence of the fully open state while inducing submaximal conductance states in single channel currents. These multiple actions are also exhibited by the scorpion calcine family toxin IpTxA, which increases full RyR openings at low nM concentrations and induces prolonged substates at low µM concentrations (21). Despite the absence of significant sequence homology (Fig. 4), the similarities between the mode of action of LITX-Lw1a and IpTxA provide functional evidence of an evolutionary link between scorpion toxins adopting the ICK and DDH folds and complement the structural and genetic support presented in our previous study (31).

The main functional divergence between the calcines and LITX is the ability of the calcines to permeate the cell membrane within the experimental constraints (23, 38). The lack of enhanced full conductance openings when LITX is applied to the trans (corresponding to the SR lumen) side of the bilayer chamber shows that LITX cannot rapidly cross the cell membrane to affect the cytosolic face of the RyR. LITX also does not form pores in the membrane, as shown by the absence of current when applied to a membrane without RyRs. It was previously noted that the calcines have a high net positive charge (+7) and that the basic residues are important for membrane permeability (39). In comparison, LITX has a lower net change of +4, which may explain its inability to pass rapidly through membranes (Fig. 4). Because the bilayer has a limited lifetime (normally <1 h), it is possible that the toxin may cross the membrane slowly. Indeed, because RyRs are located intracellularly, LITX must reach its physiological target by traversing

membranes, which may be by slow permeation. Alternatively, scorpion venoms are known to contain amphipathic helical peptides that form pores in the cell membrane, and it is possible that these pores would allow LITX to enter the cell.

**Support for the Multiple Binding Site Hypothesis for RyRs.** Like IpTxA, LITX displays multiple concentration-dependent actions on RyRs. At lower concentrations both toxins increase full openings of the RyR, and at higher concentrations they inhibit full openings and induce openings to subconductance levels and reduce the number of full conductance openings. We have previously suggested that the different actions are attributed to the toxins binding at different sites on the RyR, with binding at a high-affinity site mediating the increase in full openings and the induction of subconductance states evoked upon binding to a lower-affinity site (21).

Examination of the 3D structure of LITX revealed that the W36 side chain is exposed on the surface of the molecule and not
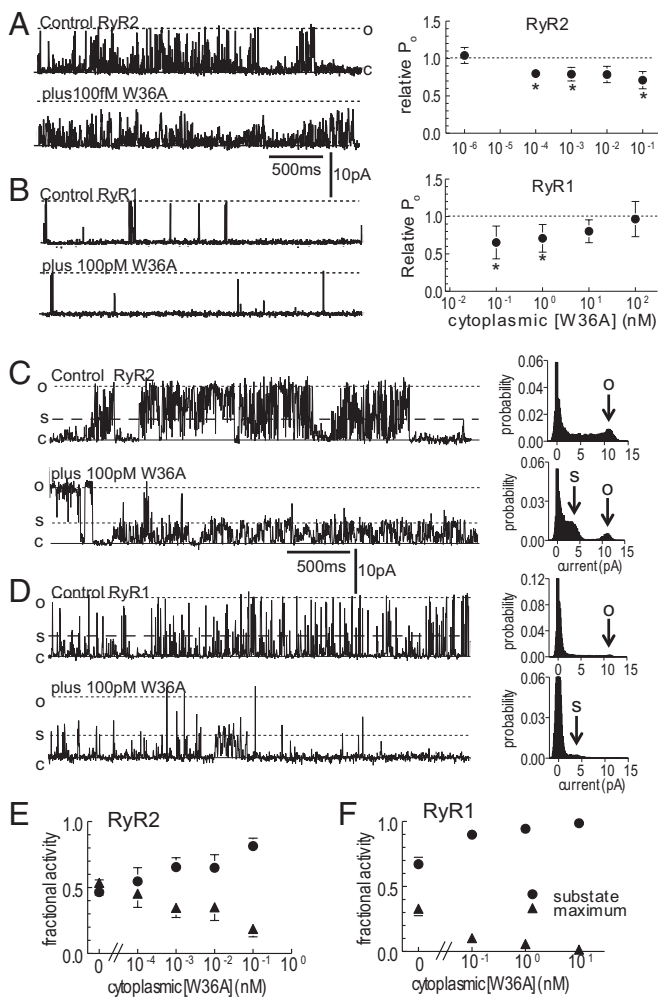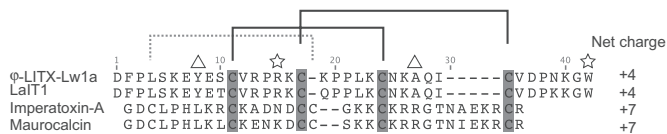
**Fig. 4.** Alignment of scorpion DDH peptides and calcines. Disulfide pairings are indicated above the sequences with square brackets, with the two solid lines indicating disulfides comprising the DDH motif and the dotted line indicating the third disulfide of the ICK motif. Triangles above the sequences highlight the Leu and Arg residues important for calcine activity; stars above the sequences highlight the Arg and Trp residues involved in scorpion DDH peptide activity at RyRs.

buried in the peptide core as would be expected for a hydrophobic residue. Moreover, tryptophan is a relatively uncommon amino acid, with tryptophan codons composing only approximately 2% of eukaryotic genes. Nevertheless, tryptophan often plays a significant role in the bioactivity of peptides and is present in 21% of protein–protein interaction hot spots (40–42). Thus, we postulated that W36 forms part of the pharmacophore and is important for activity, providing the rationale for synthesis of the W36A mutant. The C-terminal tryptophan was indeed found to be vital for the ability of LITX to increase full RyR openings, because the W36A mutant did not induce the full openings seen with the wild-type toxin. Conversely, W36 does not affect the toxin's ability to form substates, because the W36A mutant retained its substate-inducing effect. The multiple binding site hypothesis is therefore further supported by the activity of the W36A LITX mutant, which clearly demonstrates that substate induction and enhancement of full RyR openings are two discrete actions mediated by different regions of the toxin that most probably interact with distinct RyR epitopes.

[3H]Ryanodine binding assays were also included in this study. There is an average ~35–60% increase in [3H]ryanodine binding. The increases occur at the same LITX concentrations that increase channel activity (Fig. 1) and channel mean open time (Table S1). It is worth noting that Tripathy et al. (43) show a ~50–80% increase in [3H]ryanodine binding with IpTxA over much of the [$Ca^{2+}$] concentration range, emphasizing the similarity between LITX and IpTxA.

It has not been determined whether LITX and the scorpion calcines share one or more common RyR binding sites; however, their similar modes of action suggest it is possible. Mutagenesis studies of the calcines IpTxA and maurocalcine have shown that numerous basic and acidic residues contribute to the activity of these toxins (39, 44, 45). A conserved Arg at position 24 in the calcines is of particular interest because it is essential for the induction of substates, but seems to have only a small involvement in full RyR openings (38, 45). Although the role of charged residues was not investigated in this report, Arg15 was found to be functionally important in the DDH-folded LITX homolog LaIT1, with the potency of an R15A LaIT1 mutant in a cricket lethality assay reduced by 12-fold in comparison with the wild type (46). Although the molecular target of LaIT1 has not been ascertained, its homology with LITX strongly suggests it may also affect RyRs. The importance of an Arg for the activity of the calcines, and the scorpion DDH peptides suggests the two toxin classes interact with at least one common RyR binding site.

The activity of the calcines and scorpion DDH toxins cannot, however, solely be attributed to charged residues because this study highlights the functional significance of the hydrophobic W36 in LITX. Although the functionally important R24 and L7 residues of IpTxA and R15 and W36 of LITX do not align in the primary sequence (Fig. 4), it is interesting to note that the orientation and spatial positioning of the two residues are strikingly similar between the two toxins (Fig. S5). Moreover, studies of a section in the II–III loop of the dihydropyridine receptor α1 subunit known to activate RyRs have found the minimal region

**Fig. 3.** Activity of the mutant W36A toxin on RyR2 and RyR1 channels. (*A* and *B*) Cardiac RyR2 (*A*) and skeletal RyR1 (*B*); single channel currents at +40 mV (*Left*) and relative $P_o$ (*Right*), at indicated W36A concentrations. (*C* and *D*) Single RyR2 (*C*) and RyR1 (*D*) channel currents at +40 mV (*Left*) showing prolonged substate openings at indicated W36A concentrations. (*Right*) All points histograms. The arrow O indicates the full conductance level, and S points to the predominant substate current level. (*E* and *F*) The fraction of openings to submaximal levels (circles) and to the maximum conductance (triangles) for RyR2 (*E*) and RyR1 (*F*). Data are shown as mean ± 1 SEM. For visual clarity, only one error bar is shown. *Significant change at each toxin concentration.

required for activity consists of a 10-residue peptide with an N-terminal Arg and C-terminal Leu (47, 48). These observations warrant further investigation into the role of hydrophobic residues and highlight a possible relationship between an Arg and a hydrophobic residue that may be contribute to the activity of these RyR ligands. The actions of the W36A LITX mutant has hinted at the possible involvement of the C-terminal region in the initial activation of channel opening; however, additional experiments, including alanine scanning mutagenesis studies, would provide a more comprehensive examination of the structure activity relationship of RyRs and LITX.

Future investigations of LITX and the possible discovery of homologs potentially provide a basis for the development of treatments of human RyR disorders, because RyR1 mutations are associated with malignant hyperthermia and central core disease, and RyR2 mutations may play a role in stress-induced polymorphic ventricular tachycardia and arrhythmogenic right ventricular dysplasia.

## Materials and Methods

**Synthesis of Wild-Type LITX and W36A Mutant.** *Solid phase peptide synthesis.* Synthesis, oxidation, and purification of wild-type LITX were as described previously (31). The LITX W36A mutant was synthesized using Fmoc chemistry (49) on preloaded amino acid–Wang polystyrene resin on a 0.1-mmol scale. The peptide was assembled on a Symphony peptide synthesizer (Protein Technologies) with protected Fmoc-amino acid derivatives purchased from Novabiochem. The following side-chain protected amino acids were used: C(Trt), D(OtBu), E(OtBu), K(Boc), N(Trt), Q(Trt), R(Pbf), S(tBu), and Y (tBu). All other amino acids were unprotected. Fmoc was removed by treatment with 30% piperidine/*N*,*N*-dimethylformamide (DMF) (1 × 1 min, then 1 × 3 min). Couplings were performed in DMF using four equivalents of amino acid/2-(1H-benzo-triazol-1-yl)-1,1,3,3-tetramethyl uronium hexafluorophosphate/*N*,*N*-diisopropylethylamine (1:1:1) relative to resin substitution for a minimum of 15 min. Cleavage of the peptide from the resin and removal of side-chain protecting groups was achieved by treatment of the resin with TFA:H$_2$O:TIPS (9.5:2.5:2.5) at room temperature for 1 h. TFA was evaporated under nitrogen, and the cleaved peptide was precipitated then washed with cold diethyl ether, redissolved in 50% acetonitrile, and lyophilized.
*Oxidative folding.* The disulfide bonds of the W36A mutant peptide were oxidized at room temperature using 25 μM peptide dissolved in 30% isopropanol/0.1 M ammonium bicarbonate with 1:100:10 molar ratio of peptide:reduced glutathione:oxidized glutathione, pH 8.0. The oxidation mixture was left stirring for 3 d before termination of the reaction with neat TFA. The oxidized peptide was purified by reversed-phase HPLC using a Vydac C$_{18}$ column (22 × 250 mm, 10 μm) on a Waters 600 HPLC system connected to a Waters 490 Tunable Absorbance detector, and peptide was eluted from the column with an increasing concentration of solvent B (90% acetonitrile, 0.043% TFA) to solvent A (0.05% TFA). The mass of oxidized peptide was found on a matrix assisted laser desorption ionization–time of flight (MALDI-TOF) 4700 Voyager mass spectrometer. The observed [M+H]$^+$ monoisotopic mass of 4058.038 Da was in agreement with the calculated mass of 4058.044 Da.

**Structural Analysis of LITX W36A Mutant.** *Disulfide bond determination.* Because the cysteines of LITX W36A were oxidized randomly, it was necessary to determine the disulfide bond connectivity using chemical means. Fully oxidized LITX W36A was digested for 3 h at 37 °C with trypsin and digestion

fragments analyzed with MALDI-TOF mass spectrometry, as described previously (31).
*NMR spectroscopic analysis of peptide fold.* Lyophilized LITX W36A mutant was resuspended at a final concentration of 2 mM in 90% H$_2$O/10% D$_2$O, pH 3.5. A 500-μL sample solution was added to a 5-mm outer-diameter microtube (Shigemi). NMR spectra were acquired at 284 K using a 600-MHz Ultrashield spectrometer (Bruker Biospin). 2D total correlation spectroscopy (spin-lock time of 80 ms), nuclear Overhauser effect spectroscopy (mixing time of 300 ms), and double-quantum filtered correlation spectroscopy spectra were acquired. NMR spectra were analyzed manually using the TopSpin NMR software (Bruker Biospin).

**SR Isolation, Single RyR Channel Experiments, and [³H]ryanodine Binding.** Cardiac SR was prepared from sheep heart (50). Skeletal SR vesicles were isolated from the back and leg muscles of rabbits (21, 51). Ion channel currents were recorded after SR vesicle incorporation into lipid bilayers separating cis (cytoplasmic) and trans (SR lumen) solutions (21, 51). Cis Ca$^{2+}$ was buffered 1 μM with ~2 mM 1,2-bis(o-aminophenoxy)ethane-N,N,N′,N′-tetraacetic acid (BAPTA) determined using a Ca$^{2+}$ electrode. Trans Ca$^{2+}$ was 1 mM. Bilayer potential was relative to luminal solution and was changed every 30 s between +40 mV and −40 mV. Current was recorded at 5 kHz and filtered at 1 kHz. Ruthenium red was added at the end of the experiment to confirm that channels were RyRs. Single channel parameters [open probability ($P_o$), mean open time ($T_o$), and mean closed time ($T_c$)] were obtained in the usual way (33) and expressed as the value after toxin addition ($X_xT$) divided by the control value before toxin addition ($X_xC$) (i.e., $X_xT/X_xC$, so that the change in activity in each channel is expressed relative to its own internal control). [³H]ryanodine binding to SR vesicles (100 μg) was performed as described previously (52), except that the binding buffer contained 150 mM NaCl, 20 mM 3-(N-morpholino)propanesulfonic acid (Mops), 1 mM Ca$^{2+}$, and 1.59 μM BAPTA ([Ca$^{2+}$$_{free}$] = 1 μM; pH 7.4); filters were washed four times with 20 mM Mops and 150 mM NaCl; and SR vesicles were preincubated with peptides for 30 min on ice. Because SR vesicle aliquots do not contain uniform concentrations of RyR, binding data are also expressed relative to an internal control from the same vesicle aliquot. Average data for effects of the toxin relative $P_o$, and the fraction of subconductance openings were fitted with a Hill equation:

$$R = R_b + R_{max} \left\{ 1 / \left[ 1 + (AC_{50}/Tx)^H \right] \right\},$$

where $R$ is the parameter value, $R_b$ is the baseline value, $R_{max}$ is the maximum toxin-induced value, Tx is [toxin], AC$_{50}$ the [toxin] for activation to 50%, and H is the Hill coefficient.

**Statistical Analyses.** Statistical significance was evaluated by a paired or unpaired Student *t* test or analysis of variance, as appropriate. A *P* value of <0.05 was considered significant.

1. Koch GL (1990) The endoplasmic reticulum and calcium storage. *BioEssays* 12(11): 527–531.
2. Dulhunty AF, Casarotto MG, Beard NA (2011) The ryanodine receptor: A pivotal Ca2+ regulatory protein and potential therapeutic drug target. *Curr Drug Targets* 12(5):709–723.
3. Kimlicka L, Van Petegem F (2011) The structural biology of ryanodine receptors. *Sci China Life Sci* 54(8):712–724.
4. Zorzato F, et al. (1990) Molecular cloning of cDNA encoding human and rabbit forms of the Ca2+ release channel (ryanodine receptor) of skeletal muscle sarcoplasmic reticulum. *J Biol Chem* 265(4):2244–2256.
5. Otsu K, et al. (1990) Molecular cloning of cDNA encoding the Ca2+ release channel (ryanodine receptor) of rabbit cardiac muscle sarcoplasmic reticulum. *J Biol Chem* 265(23):13472–13483.
6. McPherson PS, Campbell KP (1990) Solubilization and biochemical characterization of the high affinity [3H]ryanodine receptor from rabbit brain membranes. *J Biol Chem* 265(30):18454–18460.
7. Martin C, Chapman KE, Seckl JR, Ashley RH (1998) Partial cloning and differential expression of ryanodine receptor/calcium-release channel genes in human tissues including the hippocampus and cerebellum. *Neuroscience* 85(1):205–216.
8. Ali SZ, Taguchi A, Rosenberg H (2003) Malignant hyperthermia. *Best Pract Res Clin Anaesthesiol* 17(4):519–533.
9. Priori SG, et al. (2001) Mutations in the cardiac ryanodine receptor gene (hRyR2) underlie catecholaminergic polymorphic ventricular tachycardia. *Circulation* 103(2): 196–200.
10. Ullrich ND, Valdivia HH, Niggli E (2012) PKA phosphorylation of cardiac ryanodine receptor modulates SR luminal Ca(2+) sensitivity. *J Mol Cell Cardiol* 53(1):33–42.
11. Gonzalez DR, Treuer AV, Castellanos J, Dulce RA, Hare JM (2010) Impaired S-nitrosylation of the ryanodine receptor caused by xanthine oxidase activity contributes to calcium leak in heart failure. *J Biol Chem* 285(37):28938–28945.
12. Bellinger AM, et al. (2009) Hypernitrosylated ryanodine receptor calcium release channels are leaky in dystrophic muscle. *Nat Med* 15(3):325–330.

13. Lü N, et al. (2012) Involvement of ryanodine receptors in tetanic sciatic stimulation-induced long-term potentiation of spinal dorsal horn and persistent pain in rats. *J Neurosci Res* 90(5):1096–1104.

14. Berridge MJ (2011) Calcium signalling and Alzheimer's disease. *Neurochem Res* 36(7): 1149–1156.

15. Takano K, et al. (2012) An X-linked channelopathy with cardiomegaly due to a CLIC2 mutation enhancing ryanodine receptor channel activity. *Hum Mol Genet* 21(20): 4497–4507.

16. Pessah IN, Stambuk RA, Casida JE (1987) Ca2+-activated ryanodine binding: Mechanisms of sensitivity and intensity modulation by Mg2+, caffeine, and adenine nucleotides. *Mol Pharmacol* 31(3):232–238.

17. Meissner G, el-Hashem A (1992) Ryanodine as a functional probe of the skeletal muscle sarcoplasmic reticulum Ca2+ release channel. *Mol Cell Biochem* 114(1-2):119–123.

18. Buck E, Zimanyi I, Abramson JJ, Pessah IN (1992) Ryanodine stabilizes multiple conformational states of the skeletal muscle calcium release channel. *J Biol Chem* 267(33): 23560–23567.

19. Bidasee KR, Xu L, Meissner G, Besch HR, Jr. (2003) Diketopyridylryanodine has three concentration-dependent effects on the cardiac calcium-release channel/ryanodine receptor. *J Biol Chem* 278(16):14237–14248.

20. el-Hayek R, Lokuta AJ, Arévalo C, Valdivia HH (1995) Peptide probe of ryanodine receptor function. Imperatoxin A, a peptide from the venom of the scorpion *Pandinus imperator*, selectively activates skeletal-type ryanodine receptor isoforms. *J Biol Chem* 270(48):28696–28704.

21. Dulhunty AF, Curtis SM, Watson S, Cengia L, Casarotto MG (2004) Multiple actions of imperatoxin A on ryanodine receptors: interactions with the II-III loop "A" fragment. *J Biol Chem* 279(12):11853–11862.

22. Chen L, et al. (2003) Maurocalcine and peptide A stabilize distinct subconductance states of ryanodine receptor type 1, revealing a proportional gating mechanism. *J Biol Chem* 278(18):16095–16106.

23. Schwartz EF, et al. (2009) Characterization of hadrucalcin, a peptide from *Hadrurus gertschi* scorpion venom with pharmacological activity on ryanodine receptors. *Br J Pharmacol* 157(3):392–403.

24. Ram N, et al. (2008) Design of a disulfide-less, pharmacologically inert, and chemically competent analog of maurocalcine for the efficient transport of impermeant compounds into cells. *J Biol Chem* 283(40):27048–27056.

25. Mosbah A, et al. (2000) A new fold in the scorpion toxin family, associated with an activity on a ryanodine-sensitive calcium channel. *Proteins* 40(3):436–442.

26. Daly NL, Craik DJ (2011) Bioactive cystine knot proteins. *Curr Opin Chem Biol* 15(3): 362–368.

27. Rodriguez de la Vega RC, Possani LD (2005) Overview of scorpion toxins specific for Na+ channels and related peptides: biodiversity, structure-function relationships and evolution. *Toxicon* 46(8):831–844.

28. Fry BG, et al. (2009) The toxicogenomic multiverse: Convergent recruitment of proteins into animal venoms. *Annu Rev Genomics Hum Genet* 10:483–511.

29. Zhu S, Darbon H, Dyason K, Verdonck F, Tytgat J (2003) Evolutionary origin of inhibitor cystine knot peptides. *FASEB J* 17(12):1765–1676.

30. Wang X, et al. (2000) Discovery and characterization of a family of insecticidal neurotoxins with a rare vicinal disulfide bridge. *Nat Struct Biol* 7(6):505–513.

31. Smith JJ, et al. (2011) Unique scorpion toxin with a putative ancestral fold provides insight into evolution of the inhibitor cystine knot motif. *Proc Natl Acad Sci USA* 108(26):10478–10483.

32. Copello JA, Barg S, Onoue H, Fleischer S (1997) Heterogeneity of Ca2+ gating of skeletal muscle and cardiac ryanodine receptors. *Biophys J* 73(1):141–156.

33. Tae HS, et al. (2011) Cyclization of the intrinsically disordered α1S dihydropyridine receptor II-III loop enhances secondary structure and in vitro function. *J Biol Chem* 286 (25):22589–22599.

34. Devor M (1999) Unexplained peculiarities of the dorsal root ganglion. *Pain* 6(Suppl 6): S27–S35.

35. Rush AM, Cummins TR, Waxman SG (2007) Multiple sodium channels and their roles in electrogenesis within dorsal root ganglion neurons. *J Physiol* 579(Pt 1):1–14.

36. Melli G, Hoke A (2009) Dorsal Root Ganglia Sensory Neuronal Cultures: a tool for drug discovery for peripheral neuropathies. *Expert Opin Drug Discov* 4(10):1035–1045.

37. Yotsu-Yamashita M, et al. (2004) The structure of zetekitoxin AB, a saxitoxin analog from the Panamanian golden frog *Atelopus zeteki*: A potent sodium-channel blocker. *Proc Natl Acad Sci USA* 101(13):4346–4351.

38. Estève E, et al. (2005) Transduction of the scorpion toxin maurocalcine into cells. Evidence that the toxin crosses the plasma membrane. *J Biol Chem* 280(13): 12833–12839.

39. Mabrouk K, et al. (2007) Critical amino acid residues of maurocalcine involved in pharmacology, lipid interaction and cell penetration. *Biochim Biophys Acta* 1768(10): 2528–2540.

40. Clackson T, Wells JA (1995) A hot spot of binding energy in a hormone-receptor interface. *Science* 267(5196):383–386.

41. Sun H, Greathouse DV, Andersen OS, Koeppe RE, 2nd (2008) The preference of tryptophan for membrane interfaces: insights from N-methylation of tryptophans in gramicidin channels. *J Biol Chem* 283(32):22233–22243.

42. Echols N, et al. (2002) Comprehensive analysis of amino acid and nucleotide composition in eukaryotic genomes, comparing genes and pseudogenes. *Nucleic Acids Res* 30(11):2515–2523.

43. Tripathy A, Resch W, Xu L, Valdivia HH, Meissner G (1998) Imperatoxin A induces subconductance states in Ca2+ release channels (ryanodine receptors) of cardiac and skeletal muscle. *J Gen Physiol* 111(5):679–690.

44. Lukács B, et al. (2008) Charged surface area of maurocalcine determines its interaction with the skeletal ryanodine receptor. *Biophys J* 95(7):3497–3509.

45. Seo IR, Kang DE, Song DW, Kim H (2011) Both basic and acidic amino acid residues of IpTx(a) are involved in triggering substate of RyR1. *J Biomed Biotechnol* 2011:386384.

46. Horita S, et al. (2011) Solution structure of a short-chain insecticidal toxin LaIT1 from the venom of scorpion *Liocheles australasiae*. *Biochem Biophys Res Commun* 411(4): 738–744.

47. El-Hayek R, Ikemoto N (1998) Identification of the minimum essential region in the II-III loop of the dihydropyridine receptor alpha 1 subunit required for activation of skeletal muscle-type excitation-contraction coupling. *Biochemistry* 37(19):7015–7020.

48. Casarotto MG, et al. (2000) A structural requirement for activation of skeletal ryanodine receptors by peptides of the dihydropyridine receptor II-III loop. *J Biol Chem* 275(16):11631–11637.

49. Fields GB, Noble RL (1990) Solid phase peptide synthesis utilizing 9-fluorenylmethoxycarbonyl amino acids. *Int J Pept Protein Res* 35(3):161–214.

50. Laver DR, et al. (1995) Cytoplasmic Ca2+ inhibits the ryanodine receptor from cardiac muscle. *J Membr Biol* 147(1):7–22.

51. Ahern GP, Junankar PR, Dulhunty AF (1994) Single channel activity of the ryanodine receptor calcium release channel is modulated by FK-506. *FEBS Lett* 352(3):369–374.

52. Kimura T, et al. (2005) Altered mRNA splicing of the skeletal muscle ryanodine receptor and sarcoplasmic/endoplasmic reticulum Ca2+-ATPase in myotonic dystrophy type 1. *Hum Mol Genet* 14(15):2189–2200.